The Assessment of Burn Severity and Monitoring of Recovery Process of Wildfire in Mongolia

Battsengel Vandansambuu , Byambakhuu Gantumur * , Falin Wu , Oyunsanaa Byambasuren , Sainbuyan Bayarsaikhan , Narantsetseg Chantsal , Nyamdavaa Batsaikhan , Yuhai Bao , Batbayar Vandansambuu , Munkh-Erdene Jimseekhuu

Posted Date: 1 September 2023

doi: 10.20944/preprints202309.0017.v1

Keywords: Wildfire; Burn severity; Vegetation recovery; Sentinel-2; Eastern Mongolia

Article

The Assessment of Burn Severity and Monitoring of Recovery Process of Wildfire in Mongolia

Battsengel Vandansambuu [1,2], Byambakhuu Gantumur [1,2,*], Falin Wu [3], Oyunsanaa Byambasuren [4], Sainbuyan Bayarsaikhan [1,2], Narantsetseg Chantsal [1,2], Nyamdavaa Batsaikhan [1], Yuhai Bao [5], Batbayar Vandansambuu [1,2] and Munkh-Erdene Jimseekhuu [1,2]

[1] Department of Geography, School of Arts and Sciences, National University of Mongolia, Ulaanbaatar, Mongolia; battsengel@num.edu.mn, sainbuyanb@num.edu.mn, narantsetsegch@num.edu.mn
[2] Laboratory of Geo-Informatics (GEO-iLAB), Graduate School, National University of Mongolia, Ulaanbaatar, Mongolia
[3] SNARS Laboratory, School of Instrumentation and Optoelectronic Engineering, Beihang University, Beijing, China; falin.wu@buaa.edu.cn
[4] Regional Central Asia Fire Management Resource Center, National University of Mongolia,Ulaanbaatar, Mongolia; oyunsanaa@num.edu.mn
[5] College of Geographical Science, Inner Mongolia Normal University, Hohhot, Inner Mongolia, China;
* Correspondence: byambakhuu@num.edu.mn; Tel.: +(976)-99994813

Abstract: Due to the intensification of climate change in the world, the incidence of natural disasters is increasing year by year, and monitoring, forecasting, and detecting evolution using satellite imaging technology is an important guide for remote sensing. This study aims to monitor the occurrence of fire disasters using Sentinel-2 satellite imaging technology, to determine the burned severity area with its classification and the recovery process for determining the extraordinary natural phenomena. The study area was sampled in the southeastern part of Mongolia, where have most wildfires in each year, near the Shiliin Bogd mountain in the natural steppe zone and in Bayan-Uul soum in the forest-steppe natural zone. For the methods, the NBR was used to map the area of the fire site and the classification of the burned area into 5 categories: unburned, low, moderate-low, moderate-high, and high, which are process-defined works. NDVI index was used to determine the recovery process in a timely series in the summer from April to October. In result, the burned areas were mapped from the satellite images, and the total burned area of steppe natural zone was 1164.27 km^2, of which 757.34 km^2 (65.00 percent) was low, 404.57 km^2 (34.70 percent) was moderate-low, and remaining 2.36 km^2 (0.30 percent) was moderate-high, and the total burned area of forest-steppe natural zone was 588,35 km^2, of which 158.75 km^2 (26.90 percent) was low, 297.75 km^2 (50.61 percent) was moderate-low, 131.25 km^2 (22.31 percent) was moderate-high and the remaining 0.60 km^2 (0.10 percent) was high-medium. Finally, we believe that this research is most important to helpful for emergency workers, researchers, and environmental specialists.

Keywords: wildfire; burn severity; vegetation recovery; Sentinel-2; Eastern Mongolia

1. Introduction

Wildfires are natural phenomena that have been occurring for centuries, but in recent years, their severity and frequency have increased significantly, posing substantial challenges to ecosystems and human communities. Wildfires have emerged as a global concern due to their destructive potential and wide-ranging consequences. Wildfires have been increasing last few years depending on climate changes with different natural zones by location.

Remote sensing used in satellites is most important for natural disasters including wildfires, floods, storms, and other extreme weather phenomena with acquiring pre-disasters and post-disasters [1]. Remote sensing satellite data is used for assessing damages with environmental conditions at post-disaster and risk estimation with vulnerability at pre-disaster.

Understanding and assessing wildfire severity is of utmost importance in mitigating their impact and developing effective management strategies. In recent decades, numerous regions across the world have experienced devastating wildfires, resulting in loss of lives, destruction of infrastructure, and severe ecological disturbances. The increasing severity of wildfires is attributed to various factors, including climate change, land management practices, and the accumulation of combustible vegetation. The study of wildfire severity is vital for several reasons. Firstly, severe wildfires can have long-lasting ecological impacts, altering vegetation patterns, disrupting wildlife habitats, and impairing ecosystem functioning. Secondly, they pose significant risks to human communities, affecting public health, damaging property, and causing economic losses. Thirdly, understanding wildfire severity can aid in the development of proactive strategies for fire management, including prevention, preparedness, and response.

Many studies were reviewed in the wildfire severity study field. The studies were provided by using different satellite images including optical [2–5], thermal [6,7], lidar [8], and synthetic aperture radar (SAR) [6,9,10]. Most of them were optical satellite images including MODIS data, Sentinel-2, Landsat series images, and KOMPSAT-3A [11] caused by Shortwave Infrared (SWIR) bands for the calculation. The SAR images are Sentinel-1, ALOS-2 [12], and PALSAR-2 [13]. There is a paper using lidar data that evaluates the sensitivity of full-waveform LiDAR data to estimate the severity of wildfires using a 3D radiative transfer model approach [14]. However, these all studies using LiDAR, SAR, and Thermal satellite images are estimated with optical satellite images by comparing the burned severity area and recovery processes.

Recovery of post-fire concepts is very important to this study phenomenon. There are some different approaches to define recovery processes including strong performance and suitability of the post-fire stability index [15], random forest classification models using the fire severity classes (from the Relativized Burn Ratio-RBR) as a dependent variable and 23 multitemporal vegetation indices [16], post-fire stream water responses observed in those watersheds [17], determined by multiple factors of forest's recovery rate after a wildfire, including fire severity, tree species characteristics, topography, hydrology, soil properties, and climate [18], compositing Tasseled Cap linear regression trend in a post-wildfire study site [19].

Despite extensive research on wildfires, there are still gaps in our understanding of wildfire severity, especially in specific geographic regions or under certain climatic conditions. This study aims to address the gap by focusing on the severity assessment of wildfires in the Eastern Mongolian region, which is characterized by unique topographical features and a diverse range of vegetation types. By investigating the relationship between fire behavior, fuel characteristics, and climatic factors, we seek to enhance the accuracy and effectiveness of wildfire severity assessments in this region.

Other issues are different areas and different phenomena within different natural zones in the world. We collected and reviewed a few studies in different study areas including Siberia, Russia [18,20,21], Indonesia [22], Canada [23,24], Australia [13,25–27], Spain [28], Portugal [8], Mediterranean [2,29–32], China [5,33–36], California and Alaska[37–39], US [40–44], Peru [9], Iran [45], Bolivia [46], Amazon of Brazil [47] and India [48]. The wildfire studies of each country had their characteristics.

Mongolian wildfires have increased in the past caused of climate change which is intensively influenced by natural disasters and environmental conditions. Many studies studied this case such as determining fire history from tree rings for potentials and relationships between climate change, fire and land uses [49,50], effects of wildfire on runoff generating processes in mountainous forest areas [51], wildfire and climate change study for permafrost degradation [52], and wildfire risk mapping for protected areas [53]. There are other wildfire study cases for the Mongolian Plateau such as identified drivers and spatial distributions to predict wildfire probability [54], explored growing season [55], analysis of climate-fire relationships and evaluation of the spatial change characteristics [56], and analysis of spatiotemporal wildfire pattern by satellite images [57]. Some researchers determined the cost effects of monitoring vegetation changes in steppe ecosystems [58]. Most wildfire impact cases are across borderland areas between Mongolia-Russia-China moving to disaster [59,60].

 doi:10.20944/preprints202309.0017.v1

The purpose of this study is to monitor the occurrence of fire disasters as a result of Sentinel-2 satellite imaging technology, to determine the burned area with its classification and the recovery process effects in Eastern Mongolia. This study is based on our wildfire projects and a few direct Mongolian papers which are different study areas including forest [61] and steppe [62] wildfires with their recovery effects and processes.

The remainder of this paper is structured as follows: Section 2 describes the analyzing methods for wildfire monitoring including spectral response for satellite images and statistical analyzing response; Section 3 presents a wildfire case study with study areas, data collection and processing; Section 4 discusses the results including estimation of Normalized Burn Ratio, identify burned areas, burn severity classification, and recovery after burn; the discussion is presented in Section 5; Finally, Section 6 summarizes the findings, discusses their implications, and suggests future research directions.

2. Analyzing methods for wildfire monitoring

Analyzing methods for wildfire monitoring includes two steps: spectral response for satellite images and statistical analyzing response. The spectral response for satellite images is based on NBR, dNBR, RBR, and NDVI indexes. The statistical analysis response is based on regression analysis.

2.1. Spectral response for satellite images

It is important to sensor spectral information in satellite images. Remote sensing-based burn severity indices have been developed and used due to their simple computation and direct applications for image processing. Near-infrared (NIR) and Shortwave Infrared (SWIR) bands are useful for this study.

Spatial and multitemporal NBR images are estimated proportion by difference and sum of NIR and SWIR (Band 9 and Band 12 of Sentinel-2, respectively) (Equation 1)(Figure 1). The NIR reflectance decreases owing to vegetation loss and the SWIR increases owing to a reduction in canopy humidity and shade [63].

$$NBR = \frac{(NIR - SWIR)}{(NIR + SWIR)} \tag{1}$$

The differenced NBR is estimated by NBR values of pre-fire and post-fire (Equation 2). It considers the change amounts the burned area from the unburned area.

$$dNBR = NBR_{pre-fire} - NBR_{post-fire} \tag{2}$$

The RBR is a variant of the dNBR that considers the relative amount of pre-to post-fire change by dividing dNBR by the pre-fire NBR value. This index was proposed to remove the bias due to the pre-fire vegetation type and density [64]. Equation 3 of the RBR index comes from a combination of Equation 1 and Equation 2.

$$RBR = \frac{(dNBR)}{(NBR_{pre-fire} + 1.001)} \tag{3}$$

Remotely sensed vegetation indices have also been used to analyze post-fire recovery. Normalized Difference Vegetation Index (NDVI) is useful to estimate from Sentinel-2 imagery to monitor vegetation recovery and growth after successive fires.

$$NDVI = \frac{(NIR - RED)}{(NIR + RED)} \tag{4}$$

The geographical scales (i.e., geometry, pixel size, and projection) of all estimated variable files should be in the same scales for the next statistical analysis response.

Preprints (www.preprints.org) | NOT PEER-REVIEWED | Posted: 1 September 2023 doi:10.20944/preprints202309.0017.v1

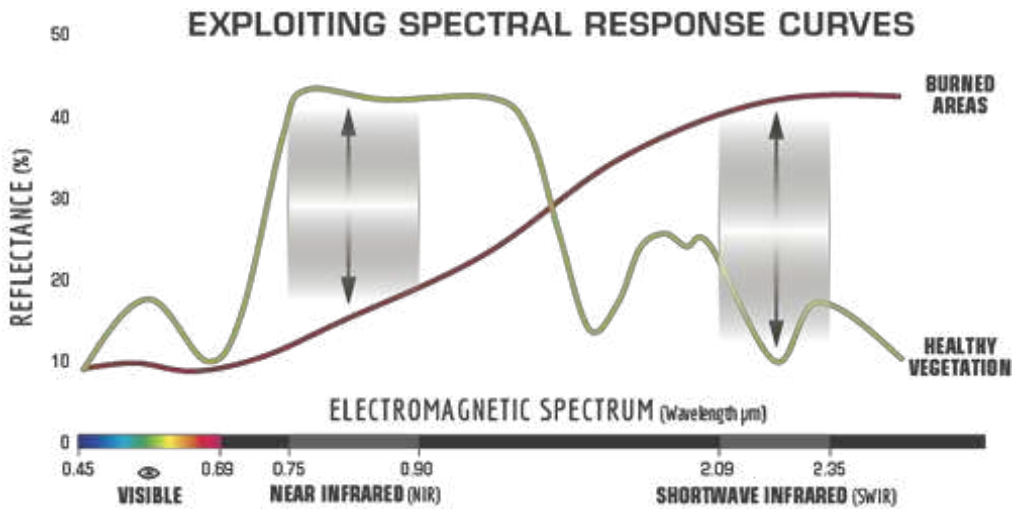

Figure 1. Healthy plant species reflect more energy in NIR but weakly in SWIR. This spectral characteristic is useful for detecting burned areas such as dead soil/plant material on forest floors. Source: US Forest Service.

2.2. Statistical analysis response

Regression analysis and scatter plots have been used for statistical analysis of responses. In this case, we tried to determine the phenomenon that the recovery processes are dependent on NBR from wildfire start to end of recovery.

The correlation and regression analysis are obtained in this statistical method for the relationship between the indicator factors [65]. Pearson's correlation coefficient (r) indicates the correlation between two variables that determination by

$$r_{xy} = \frac{\sum_{i=1}^{n}(x_i - \bar{x})(y_i - \bar{y})}{\sqrt{\sum_{i=1}^{n}(x_i - \bar{x})^2}\sqrt{\sum_{i=1}^{n}(y_i - \bar{y})^2}} \quad (5)$$

where n is the sample size; x_i, y_i are the individual sample points indexed with i; $\bar{x} = \sum_{i=1}^{n} x_i$ (the sample mean) and analogously for $\bar{y}$.

The regression analysis was used by linear regression and scatter plot graphs that were pointed in intercept and slope. It demonstrates that scattering distributions are changing the shapes and locations. These describe the phenomena that we want to see. A correlation and regression analysis were used to determine the relationships between NBR and NDVI during the recovery process.

3. Wildfire case study

3.1. Study Areas

Shiliin Bogd Mountain is in Eastern Mongolia (45˚20′ – 45˚40′ N and 114˚20′ – 115˚20′ E; Figure 2-1) in Sukhbaatar province on the border of Mongolia and China. The burned area is calculated at 6879.67 km² and elevation is between 1300 and 1800 m. The average annual temperature and precipitation of the whole range are 1.5-1.7˚C (mean maximum 30˚C in July, mean minimum -32.5˚C in January) and 200.6 mm. Precipitation follows a bimodal distribution, with maxima in June–September and November–February. The rainiest months are July and August, with 150 mm on average, and the snowiest months are December and January, with 40 mm on average. Additionally, the driest present an increase in March to May, and September to November.

Preprints (www.preprints.org) | NOT PEER-REVIEWED | Posted: 1 September 2023 doi:10.20944/preprints202309.0017.v1

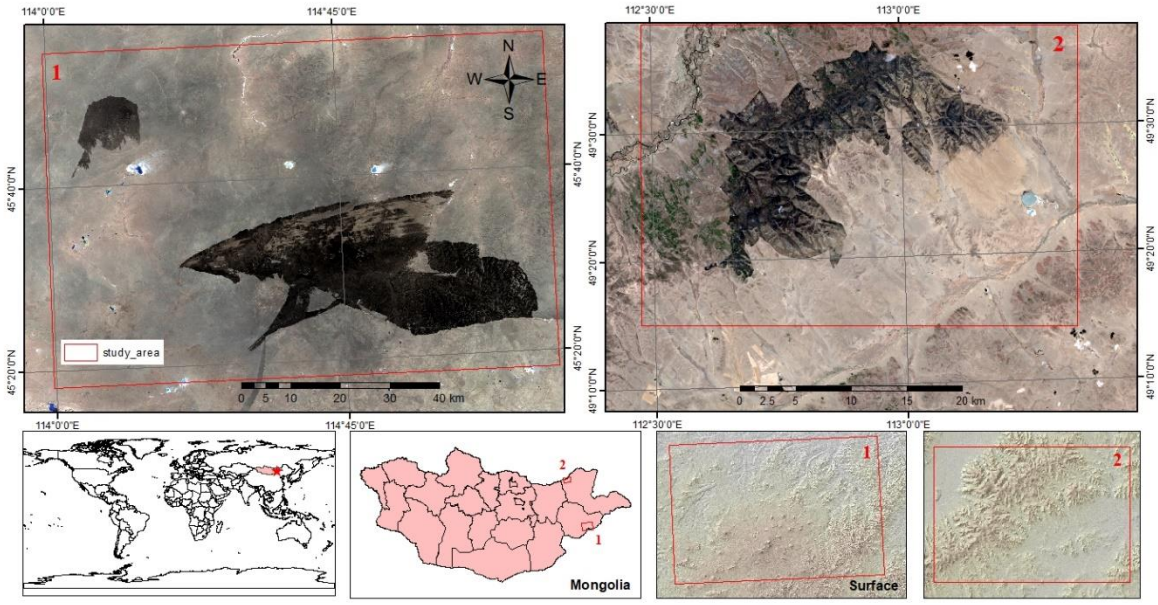

Figure 2. The sampled burned areas at Shiliin bogd mountain and sub-provinces of Bayan-Uul and Bayandun in Eastern Mongolia. Sentinel-2 satellite imagery on April 20, 2021, and May 01, 2020.

The area of provinces of Bayan-Uul and Bayandun is in North-Eastern Mongolia (49˚15′ – 49˚40′ N and 112˚30′ – 113˚30′ E; Figure 2-2) in Dornod province on the border of Mongolia and Russia. The burned area is calculated in 588.35 km² and elevation is between 1100 and 1500 m. The average annual temperature and precipitation of the whole range are -1- 0.7˚C (mean maximum 20˚C in July, mean minimum -22˚C in January) and 250-400 mm. Precipitation follows a bimodal distribution, with maxima in June–September and November–February. The rainiest months are July and August, with 300 mm on average, and the snowiest months are December and January, with 70 mm on average. Additionally, the driest present an increase in March to May, and September to November.

The first sampled area is at old aged volcano mountains which is one side of the steppe of natural zones (Figure 3). The second sampled study area is a beautiful wildland that is on the other side of Khentii mountains and contains in forest-steppe of natural zones (experimental views in Figure 4). Therefore, those two sampled areas are the roles of two different natural zones of forest-steppe and steppe. This study imagines estimating the results of wildfires in different places and compares two different kinds of wildfires in natural zones.

Figure 3. The experimental views of the sampled area at Shiliin bogd mountain.

Preprints (www.preprints.org) | NOT PEER-REVIEWED | Posted: 1 September 2023 doi:10.20944/preprints202309.0017.v1

Figure 4. The experimental views of the sampled area in the province of Bayan-Uul and Bayandun.

Wildfires happen in the dry seasons of spring and fall of the year especially in the border zone of Mongolia. There are two kinds of legitimacy in this study. One of these wildfires comes from the Russian side. Another one is gone to the Chinese border side (Figure 2).

3.2. Data collection and processing

The Sentinel-2 satellite series has continually observed Earth since 2015 and accumulated an enormous number of time series images. Table 1 demonstrates the characteristics of the Sentinel-2 satellite image.

Table 1. Spectral bands characteristics and spatial resolution of Sentinel-2A MSI sensor. Source: ESA, 2015.

	Spectral Band	Spatial resolution (nm)	Centre Wavelength (nm)	Band Width (nm)
B1	Coastal aerosol	60	443	20
B2	Blue	10	494	65
B3	Green	10	560	35
B4	Red	10	665	30
B5	Vegetation red edge	20	704	15
B6	Vegetation red edge	20	740	15
B7	Vegetation red edge	20	781	20
B8	NIR	10	834	115
B8a	Narrow NIR or NIR 2	20	864	20
B9	Water vapour	60	944	20
B10	SWIR – Cirrus	60	1375	30
B11	SWIR 1	20	1612	90
B12	SWIR2	20	2185	185

Sixteen cloud-free Sentinel-2 of 2A and 2B images have been selected for this study, which were collected from April to September 2020 and 2021 (Table 2), respectively, and were acquired from ESA Sci-Hub. The Sentinel-2 satellite images were found better than Landsat-8 images. Therefore, Sentinel-2 was selected for image processing and demonstrated better information.

In addition, a time series of satellite images is better to show from April to September of each year for two sampled areas.

Table 2. Data collection of Sentinel-2 satellite images.

Date of 1st sampled area	Date of 2nd sampled area
April 5, 2021	April 11, 2020
April 20, 2021	April 16, 2020
May 5, 2021	April 23, 2020
May 15, 2021	May 01, 2020

Preprints (www.preprints.org) | NOT PEER-REVIEWED | Posted: 1 September 2023 doi:10.20944/preprints202309.0017.v1

July 19, 2021	May 08, 2020
August 18, 2021	June 20, 2020
September 17, 2021	July 22, 2020
September 27, 2021	August 21, 2020

4. Results

The assessment and monitoring results of burn severity and recovery process of wildfire in Mongolia are analyzed in this section. Section 4.1 analyzed the defining normalized burn ratio by spectral bands. Section 4.2 identified the burned areas in the study sampled areas; Section 4.3 analyzed burn severity classification; Section 4.4 monitored recovery processes post-fire.

4.1. Estimation of Normalized Burn Ratio

NBR was estimated on bands of satellite images which are time ranged from spring to fall. The NBR change of images of time series was demonstrated in Figure 5 which was calculated by Equation 1.

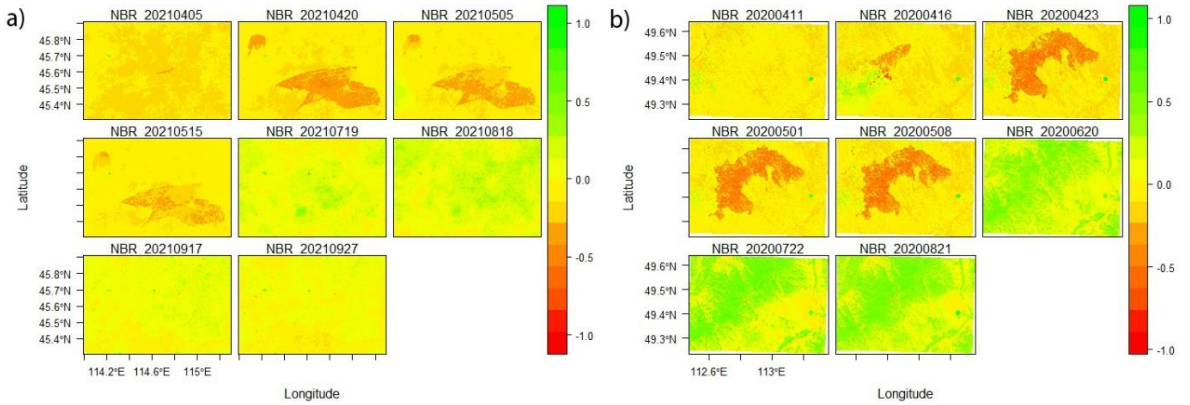

Figure 5. The estimated images of NBR which is compared on time series. .

When values of raster images were decreasing, it was colored red color. It means the burned level is the highest. When values are increasing, the color is going to green. It means the burned level is lower.

The index of NBR is used to determine the burned area for the next.

4.2. Identify burned areas

NBR indices of before and after were used to identify burned areas for the RBR index. In the first study area, satellite images were selected on April 5, 2021, and April 20, 2021. In the second study area, satellite images were selected on April 11 and May 01, 2020, respectively. There are two satellite images which were between April 11, and May 01 of 2020. Because some clouds were on the images. It brings some difficulties in estimating the results for the dNBR index.

The index of dNBR is calculated by making lower adjustments to NBR before the fire occurs to avoid miscalculation of the equation [66]. Figure 6 demonstrates the RBR index, which ranges coefficients between -1.37 and 1.19. It is colored values from blue to red. Positive values ranged from yellow color to red color, which means estimation of burned area. Negative values ranged from blue color to yellow color which means estimation of unburned area.

As shown in Figure 6, the burned area is expected to reach 1164.27 square km in the first image and 588,35 square km in the second image.

Burn severity classification was determined in the next chapter.

Preprints (www.preprints.org) | NOT PEER-REVIEWED | Posted: 1 September 2023 doi:10.20944/preprints202309.0017.v1

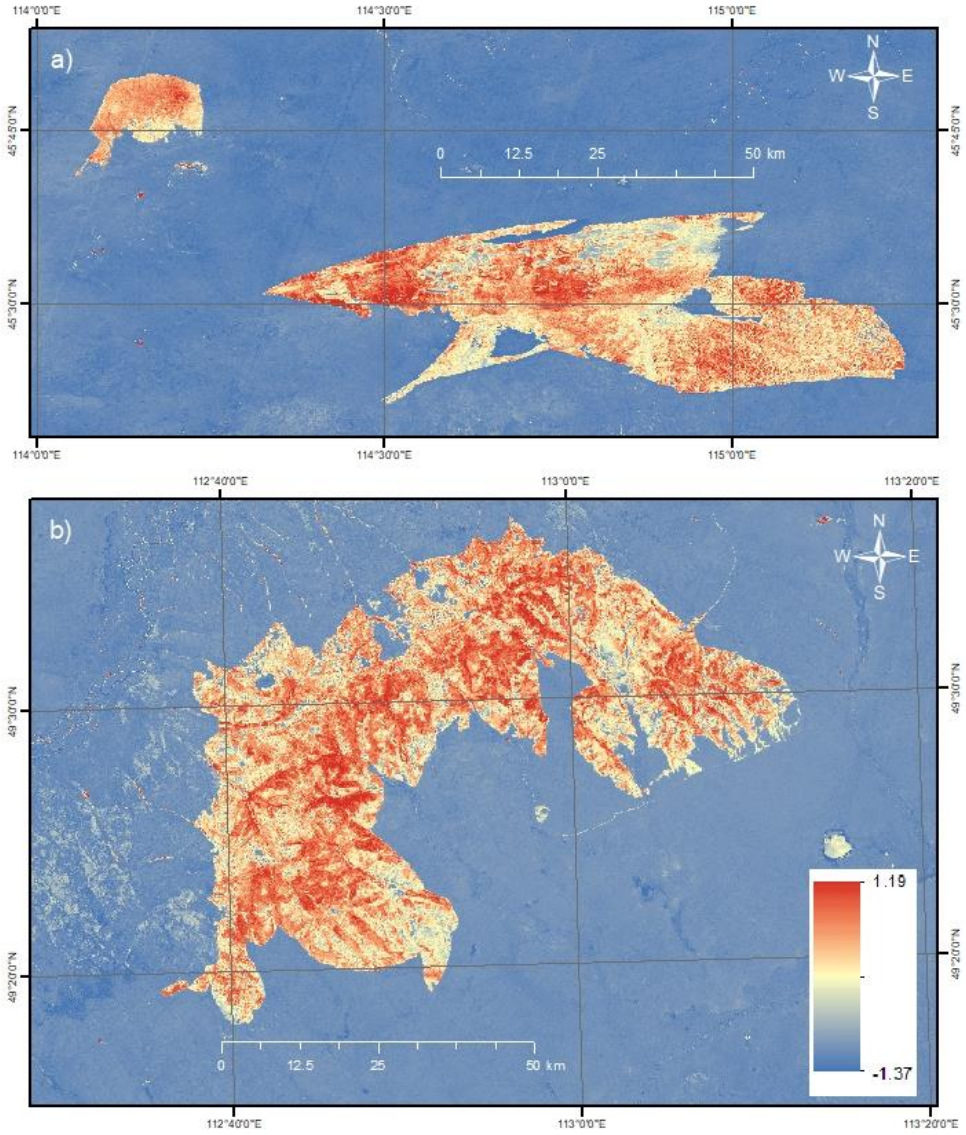

Figure 6. The estimation of dNBR which are defined damaged area on two sampled study area.

4.3. Burn severity classification

In the third proposed result, the burn severity is classified by RBR values of pre-fire and post-fire. It helps aid in emergencies and to assess the recovery process post-fire. The burn severity is suggested by the United States Geological Survey (USGS), and it is shown in Table 3.

Table 3. Burn severity classification criteria table (USGS).

Severity level	dNBR range (scaled by 10^3)	dNBR range (not scaled)
Enhanced regrowth, high (post-fire)	-500 to -251	-0.500 to -0.251
Enhanced regrowth, low (post-fire)	-250 to -101	-0.250 to -0.101
Unburned	-100 to +99	-0.100 to +0.99
Low severity	+100 to +269	+0.100 to +0.269
Moderate-low severity	+270 to +439	+0.270 to +0.439
Moderate-high severity	+440 to +659	+0.440 to +0.659
High severity	+660 to +1300	+0.660 to +1.300

Preprints (www.preprints.org) | NOT PEER-REVIEWED | Posted: 1 September 2023 doi:10.20944/preprints202309.0017.v1

After the estimation of dNBR, the RBR is calculated by Equation 3 using the ratio of dNBR and $NBR_{pre\text{-}fire}$. Then raster image of RBR was reclassified by values of dNBR range. It is demonstrated in Table 3. The RBR estimation raster images are shown in Figure 7. When RBRs of study areas are estimated in Figure 7, a comparison of RBR was differenced forest-steppe and steppe areas by colors. Forest-steppe area was burned more than the steppe area.

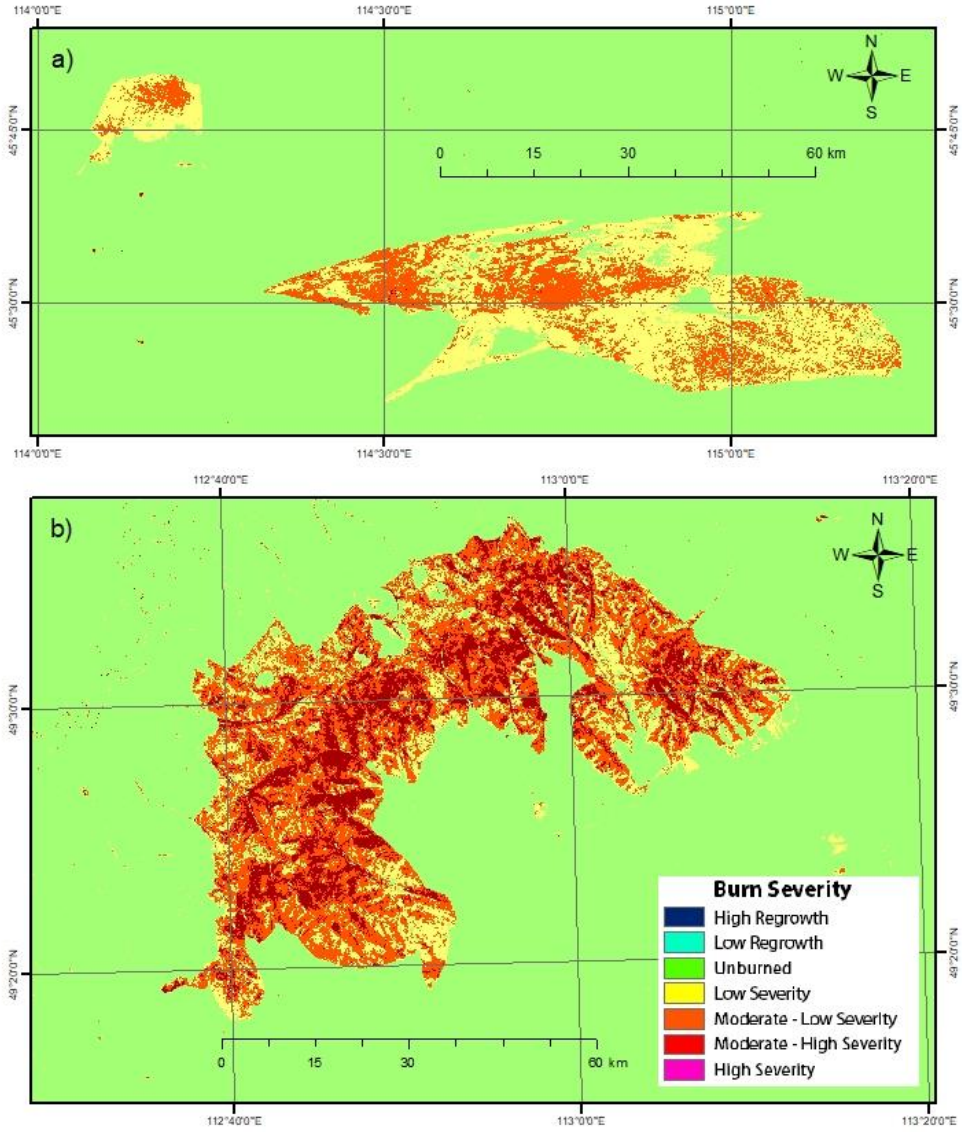

Figure 7. The classification of burn severity on two sampled study areas.

The burned total area was divided into 757.34 km² (low severity - 65.00 percent), 404.57 km² (moderate-low severity - 34.70 percent), and 2.36 km² (moderate-high severity-0.3 percent) in the first sampled area of steppe natural zone at Figure 7-a. The other burned total area was divided into 158.75 km² (low severity - 26.90 percent), 297.75 km² (moderate-low severity - 50.61 percent), 131.25 km² (moderate-high severity - 22.31 percent), and 0.60 km² (high severity - 0.10 percent) in second sampled area of forest-steppe natural zone at Figure 7-b.

In this result of figures, the forest and mountain areas are burned more deeply than the steppe area. Because it depends on wind speed.

Preprints (www.preprints.org) | NOT PEER-REVIEWED | Posted: 1 September 2023 doi:10.20944/preprints202309.0017.v1

4.4. Recovery process after burn

NDVI was estimated on RED and NIR bands of satellite images which time ranged from spring to fall. The NBR change of images of time series was demonstrated in Figure 8 which was calculated by Equation 4.

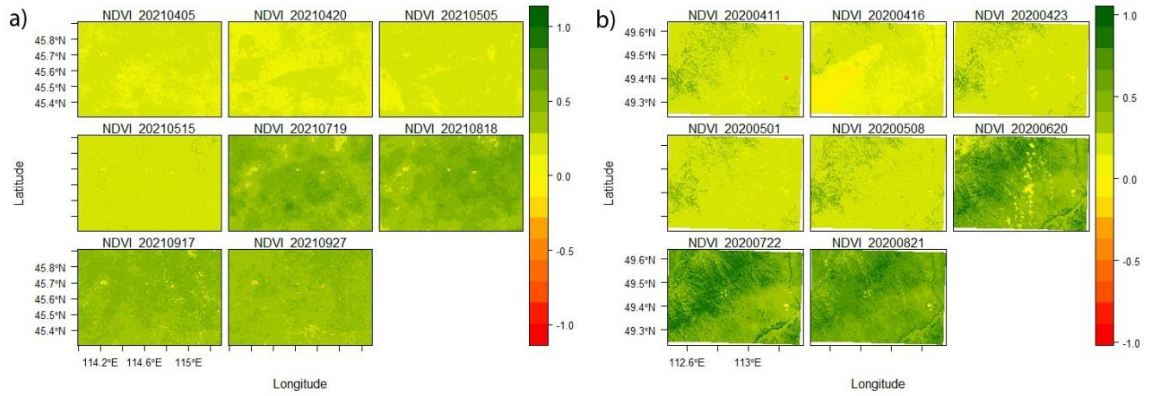

Figure 8. The change detection of two sampled areas (a. Shiliin bogd mountain area of steppe and b. forest area on sub-provinces of Bayan-Uul and Bayandun) on time series.

When values of raster images were decreasing, it was colored red color. It means vegetation distribution is the lowest. When values were increasing, the color was going to dark green. It means vegetation is distributed higher. Figure 8 demonstrates vegetation covers which are compared between the two sampled study areas. The vegetation distribution level of the forest area is higher than steppe area. In these two images, there aren't worse influences on nature after burning. The vegetation has recovered better than before.

In the special phenomena, vegetation grows during the time from spring to autumn for passing the years. The vegetation dries every autumn season for years. It accumulates a lot on the ground. Therefore, wildfire cleans to burn all accumulated and dried vegetation. The best thing is that nature cleans itself and the worst thing is human settlement reached damage for wildfire. But Mongolian wildfires are not like Australia, Russia, and the United States, they depend on wind speed and burn only the skin of trees. Damages are not 100 percent of burning (Figure 9). This is Mongolian wildfires different from other country's wildfires.

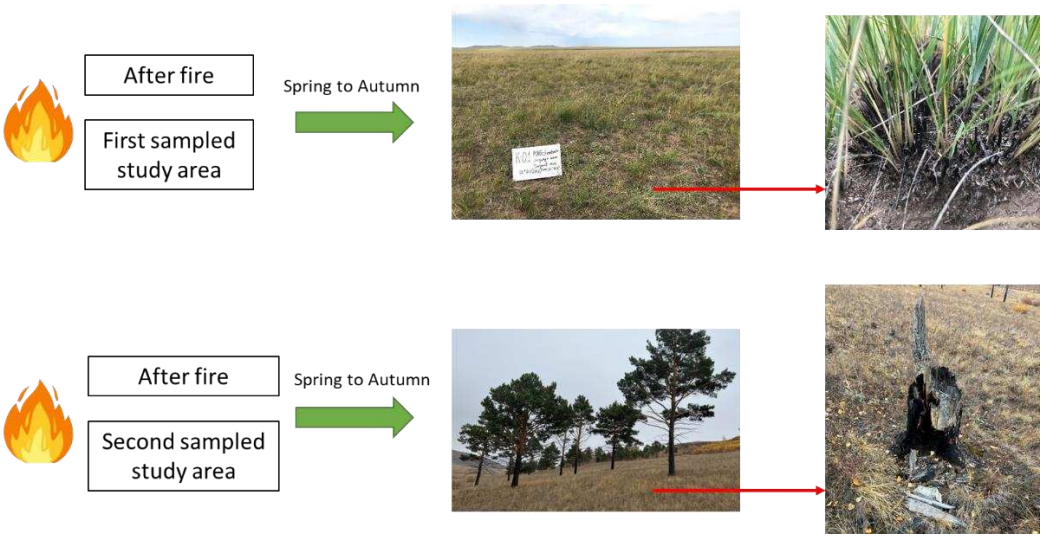

Figure 9. Experimental views of the recovering process at each sampled area.

Preprints (www.preprints.org) | NOT PEER-REVIEWED | Posted: 1 September 2023 doi:10.20944/preprints202309.0017.v1

5. Discussion

First, RBR of wildfire severity results and NDVI of vegetation recovery process results have been estimated. These indexes are during the vegetation recovery process from the spring to autumn seasons. It means recovering processes and collected data in time series. Data of RBR and NDVI are at the same time. Therefore, the relationships between raster images of RBR and NDVI were calculated in Figures 10 and 11 by the separate natural zones including sampled steppe and forest-steppe areas. We will the discussion on these relationships, which have particular natural laws on each figure.

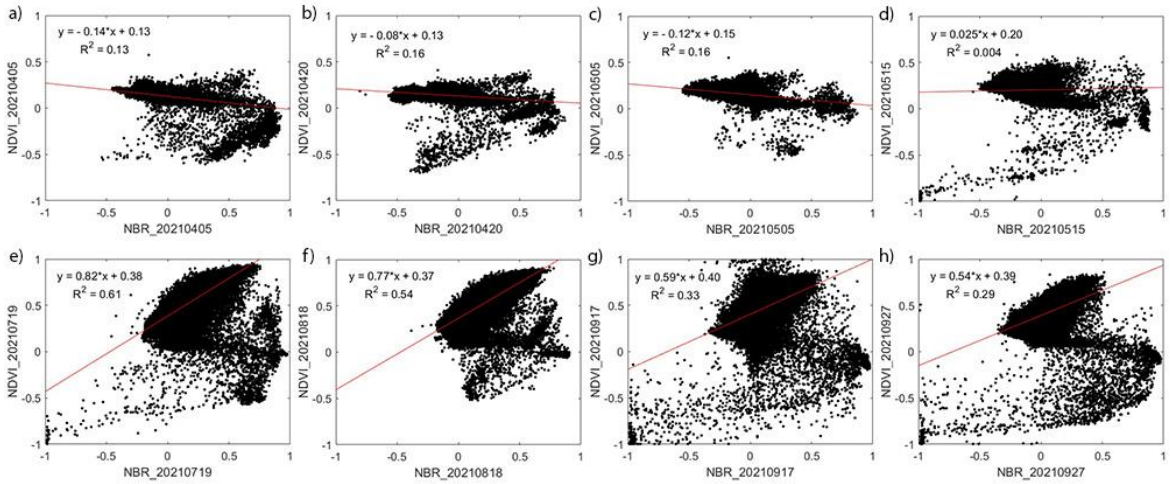

Figure 10. The relationships on scatter plots between NDVI and NBR in the recovery process in the first sampled steppe area.

Figure 10 illustrates the scatter plot of the recovery processes of the first sampled steppe area. It is shown that the related scattering distributions, when were at April 5, April 20, May 5, May 15, July 19, August 18, September 17, and September 27 in 2021. The burned date was exactly April 18, 2021. There are the coefficients of intercepts and slopes, which were 0.13, 0.13, 0.15, 0.20, 0.38, 0.37, 0.40, and 0.39 with increased, which were -0.14, 0.08, -0.12, 0.025, 0.82, 0.77, 0.59, and 0.54, respectively.

In addition, correlation coefficients are calculated in Figure 10, which were 0.13, 0.16, 0.16, 0.004, 0.61, 0.54, 0.33, and 0.29, respectively. The first three plots have a negative correlation with healthy vegetation covers. But the exact burning date plot is in Figure 10-b. Therefore, it is lower than beside plots. Then, it is increased till the autumn season. When the last 2 month's vegetation is getting yellow-colored in satellite images, the correlation is decreased. Dates were in September.

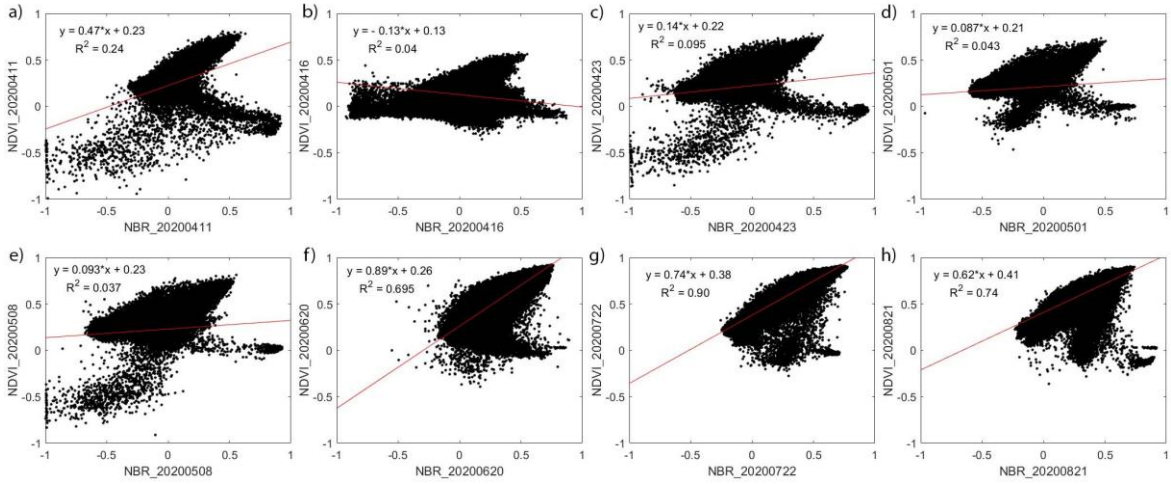

Figure 11. The relationships on scatter plots between NDVI and NBR in the recovery process in the first sampled forest-steppe area.

Figure 11 illustrates the scatter plot of the recovery processes of the first sampled forest-steppe area. It is shown that the related scattering distributions, when were at April 11, April 16, April 23, May 1, May 8, June 20, July 22, and August 21 in 2020. Burned date was started from April 15 and continued to May 1, 2021. There are the coefficients of intercepts and slopes, which were 0.23, 0.13, 0.22, 0.21, 0.23, 0.26, 0.38, and 0.41 with increased, which were 0.47, -0.13, 0.14, 0.087, 0.093, 0.89, 0.74, and 0.62 with increased, respectively.

In addition, correlation coefficients are calculated in Figure 11, which were 0.24, 0.04, 0.095, 0.043, 0.037, 0.69, 0.90, and 0.74, respectively. The second plot has a negative correlation with healthy vegetation covers. But the exact burning date plot is in Figure 11-b. Therefore, it is negative. Then, it is increased till the autumn season. When last month's vegetation is getting yellow-colored in satellite images, the correlation is decreased. Dates were at the end of August.

The plots of each figure demonstrate that the difference between the plots of Figure 10 is lighter scattered than the plots of Figure 11. This means the forest-steppe natural zone has more fire severity than the steppe natural zone. Both are recovered 100 percent at the end of the summer season itself and naturally.

6. Conclusions

Finally, we conclude that Mongolian wildfires are increasingly caused by relating with climate change. But there are interesting phenomena of wildfires in Natural zones. Site selection was demonstrated in two different natural zones including forest-steppe and steppe areas. The wildfire severity of the forest-steppe zone is higher than the wildfire severity of the steppe zone. The wildfires of the steppe area were influenced by winds. The winds are stronger than the wind of forest-steppe areas. Therefore, wildfires in the steppe are burning light severity.

In the recovery process, there are no effects on the sites with vegetation growing. The quality of vegetation cover has grown better than before the wildfire. But the cover percentage is lighter than before the wildfire. Only tree bark and skin are affected by wildfire in forest-steppe areas. Therefore, wildfire is damaged in estimation after recovery processes. But if there was human property in the wildfire process, damages would be increased. Wildfire hazards are not very harmful in Mongolia.

This research has innovated successful new findings in Mongolian wildfire research. In addition, the next research will be based on this research and continue this wildfire study.

Author Contributions: Conceptualization, B.V., B.G., and Y.B.; methodology, B.G., and N.C; validation, B.V., N.B., and O.B.; formal analysis, B.G. and S.B.; investigation, B.V. and Ba.V.; resources and curation, N.C. Ba.V. and M.J.; writing—original draft preparation, B.G., and F.W.; writing—review and editing, F.W.; visualization, N.C. and S.B.; supervision, B.V.; project administration, B.V. and B.G. All authors have read and agreed to the published version of the manuscript.

Funding: This research was funded by the National Natural Science Foundation of China (41861021) and the Mongolian Foundation for Science and Technology. Also, we have another project named "Wildfire Monitoring of Natural Disaster and Its Risk Assessment Using Remote Sensing Methods in Mongolia" (APSCO/PO&DS/1st BATCH OF DSSP APPLICATION/IMP_C_008) which was funded by the Asia-Pacific Space Cooperation Organization (APSCO). The National University of Mongolia (NUM) is supporting to implementation of a project (P2022-4261) in the field.

Acknowledgments: We thank Copernicus Open Access Hub of ESA, EarthExplorer of USGS, and the Data Sharing Service Platform (DSSP) of APSCO for accessible data products. We also thank to National University of Mongolia (NUM) for all its support.

Conflicts of Interest: The authors declare no conflict of interest.

References

1. Bello, O.M. and Y.A. Aina, *Satellite Remote Sensing as a Tool in Disaster Management and Sustainable Development: Towards a Synergistic Approach.* Procedia - Social and Behavioral Sciences, 2014. **120**: p. 365-373.

2. Alcaras, E., et al., *Normalized Burn Ratio Plus (NBR plus): A New Index for Sentinel-2 Imagery.* Remote Sensing, 2022. **14**(7).
3. Amos, C., G.P. Petropoulos, and K.P. Ferentinos, *Determining the use of Sentinel-2A MSI for wildfire burning & severity detection.* International Journal of Remote Sensing, 2019. **40**(3): p. 905-930.
4. Brovkina, O., et al., *Monitoring of post-fire forest scars in Serbia based on satellite Sentinel-2 data.* Geomatics Natural Hazards & Risk, 2020. **11**(1): p. 2315-2339.
5. Cai, L.Y. and M. Wang, *Is the RdNBR a better estimator of wildfire burn severity than the dNBR? A discussion and case study in southeast China.* Geocarto International, 2022. **37**(3): p. 758-772.
6. Abdikan, S., et al., *Burned Area Detection Using Multi-Sensor SAR, Optical, and Thermal Data in Mediterranean Pine Forest.* Forests, 2022. **13**(2).
7. Safder, Q., et al., *BA_EnCaps: Dense Capsule Architecture for Thermal Scrutiny.* Ieee Transactions on Geoscience and Remote Sensing, 2022. **60**.
8. Fernandez-Guisuraga, J.M. and P.M. Fernandes, *Using Pre-Fire High Point Cloud Density LiDAR Data to Predict Fire Severity in Central Portugal.* Remote Sensing, 2023. **15**(3).
9. Alarcon-Aguirre, G., et al., *Burn Severity Assessment Using Sentinel-1 SAR in the Southeast Peruvian Amazon, a Case Study of Madre de Dios.* Fire-Switzerland, 2022. **5**(4).
10. Chhabra, A., et al., *RADAR-Vegetation Structural Perpendicular Index (R-VSPI) for the Quantification of Wildfire Impact and Post-Fire Vegetation Recovery.* Remote Sensing, 2022. **14**(13).
11. Lee, S.M. and J.C. Jeong, *Forest Fire Severity Classification Using Probability Density Function and KOMPSAT-3A.* Korean Journal of Remote Sensing, 2019. **35**(6): p. 1341-1350.
12. Fernandez-Guisuraga, J.M., et al., *ALOS-2 L-band SAR backscatter data improves the estimation and temporal transferability of wildfire effects on soil properties under different post-fire vegetation responses.* Science of the Total Environment, 2022. **842**.
13. Fernandez-Carrillo, A., L. McCaw, and M.A. Tanase, *Estimating prescribed fire impacts and post-fire tree survival in eucalyptus forests of Western Australia with L-band SAR data.* Remote Sensing of Environment, 2019. **224**: p. 133-144.
14. Garcia, M., et al., *Evaluating the potential of LiDAR data for fire damage assessment: A radiative transfer model approach.* Remote Sensing of Environment, 2020. **247**.
15. Gibson, R.K., et al., *The post-fire stability index; a new approach to monitoring post-fire recovery by satellite imagery.* Remote Sensing of Environment, 2022. **280**.
16. Maxwald, M., et al., *Analyzing Fire Severity and Post-Fire Vegetation Recovery in the Temperate Andes Using Earth Observation Data.* Fire-Switzerland, 2022. **5**(6).
17. Rust, A.J., et al., *Evaluating the factors responsible for post-fire water quality response in forests of the western USA.* International Journal of Wildland Fire, 2019. **28**(10): p. 769-784.
18. Shvetsov, E.G., et al., *Assessment of post-fire vegetation recovery in Southern Siberia using remote sensing observations.* Environmental Research Letters, 2019. **14**(5).
19. Kim, S.I., D.S. Ahn, and S.C. Kim, *RGB Composite Technique for Post Wildfire Vegetation Monitoring Using Sentinel-2 Satellite Data.* Korean Journal of Remote Sensing, 2021. **37**(5): p. 939-946.
20. Talucci, A.C., et al., *Evaluating Post-Fire Vegetation Recovery in Cajander Larch Forests in Northeastern Siberia Using UAV Derived Vegetation Indices.* Remote Sensing, 2020. **12**(18).
21. Barrett, K., et al., *Postfire recruitment failure in Scots pine forests of southern Siberia.* Remote Sensing of Environment, 2020. **237**.
22. Sutomo and E.J.B. van Etten, *Fire Impacts and Dynamics of Seasonally Dry Tropical Forest of East Java, Indonesia.* Forests, 2023. **14**(1).
23. Gerrand, S., et al., *Partitioning carbon losses from fire combustion in a montane Valley, Alberta Canada.* Forest Ecology and Management, 2021. **496**.
24. Wang, W.W., et al., *Burn Severity in Canada's Mountain National Parks: Patterns, Drivers, and Predictions.* Geophysical Research Letters, 2022. **49**(12).
25. Gibson, R.K. and S. Hislop, *Signs of resilience in resprouting Eucalyptus forests, but areas of concern: I year of post-fire recovery from Australia's Black Summer of 2019-2020.* International Journal of Wildland Fire, 2022. **31**(5): p. 545-557.
26. Ndalila, M.N., et al., *Evolution of a pyrocumulonimbus event associated with an extreme wildfire in Tasmania, Australia.* Natural Hazards and Earth System Sciences, 2020. **20**(5): p. 1497-1511.
27. Shah, S.U., et al., *Relating McArthur fire danger indices to remote sensing derived burned area across Australia.* International Journal of Wildland Fire, 2023. **32**(2): p. 133-148.
28. Fernandez, C., et al., *Exploring the use of spectral indices to assess alterations in soil properties in pine stands affected by crown fire in Spain.* Fire Ecology, 2021. **17**(1).
29. Domingo, D., et al., *Fuel Type Classification Using Airborne Laser Scanning and Sentinel 2 Data in Mediterranean Forest Affected by Wildfires.* Remote Sensing, 2020. **12**(21).
30. Balde, B., et al., *The relationship between fire severity and burning efficiency for estimating wildfire emissions in Mediterranean forests.* Journal of Forestry Research, 2023.

31. Adaktylou, N., D. Stratoulias, and R. Landenberger, *Wildfire Risk Assessment Based on Geospatial Open Data: Application on Chios, Greece.* Isprs International Journal of Geo-Information, 2020. **9**(9).
32. Quintano, C., et al., *Burn Severity and Post-Fire Land Surface Albedo Relationship in Mediterranean Forest Ecosystems.* Remote Sensing, 2019. **11**(19).
33. Cao, X.C., et al., *Characteristics and predictive models of hillslope erosion in burned areas in Xichang, China, on March 30, 2020.* Catena, 2022. **217**.
34. Li, W.H., et al., *Predictive model of spatial scale of forest fire driving factors: a case study of Yunnan Province, China.* Scientific Reports, 2022. **12**(1).
35. Li, X.Y., et al., *Effects of fire history on thermal regimes of permafrost in the northern Da Xing'anling Mountains, NE China.* Geoderma, 2022. **410**.
36. Shirazi, Z., L. Wang, and V.G. Bondur, *Modeling Conditions Appropriate for Wildfire in South East China - A Machine Learning Approach.* Frontiers in Earth Science, 2021. **9**.
37. Keeley, J.E., T.J. Brennan, and A.D. Syphard, *The effects of prolonged drought on vegetation dieback and megafires in southern California chaparral.* Ecosphere, 2022. **13**(8).
38. Madani, N., et al., *The Impacts of Climate and Wildfire on Ecosystem Gross Primary Productivity in Alaska.* Journal of Geophysical Research-Biogeosciences, 2021. **126**(6).
39. Mathews, L.E.H. and A.M. Kinoshita, *Urban Fire Severity and Vegetation Dynamics in Southern California.* Remote Sensing, 2021. **13**(1).
40. Ball, G., et al., *Wildfires increasingly impact western US fluvial networks.* Nature Communications, 2021. **12**(1).
41. Balch, J.K., et al., *FIRED (Fire Events Delineation): An Open, Flexible Algorithm and Database of US Fire Events Derived from the MODIS Burned Area Product (2001-2019).* Remote Sensing, 2020. **12**(21).
42. Hammond, D.H., et al., *Boreal forest vegetation and fuel conditions 12 years after the 2004 Taylor Complex fires in Alaska, USA.* Fire Ecology, 2019. **15**(1).
43. Moris, J.V., et al., *Using a trait-based approach to asses fire resistance in forest landscapes of the Inland Northwest, USA.* Landscape Ecology, 2022. **37**(8): p. 2149-2164.
44. Palaiologou, P., et al., *Locating Forest Management Units Using Remote Sensing and Geostatistical Tools in North-Central Washington, USA.* Sensors, 2020. **20**(9).
45. Gholamrezaie, H., et al., *Automatic Mapping of Burned Areas Using Landsat 8 Time-Series Images in Google Earth Engine: A Case Study from Iran.* Remote Sensing, 2022. **14**(24).
46. Maillard, O., et al., *Phenology Patterns and Postfire Vegetation Regeneration in the Chiquitania Region of Bolivia Using Sentinel-2.* Fire-Switzerland, 2022. **5**(3).
47. Santana, N.C., et al., *Comparison of Post-fire Patterns in Brazilian Savanna and Tropical Forest from Remote Sensing Time Series.* Isprs International Journal of Geo-Information, 2020. **9**(11).
48. Kale, M.P., et al., *Forecasting wildfires in major forest types of India.* Frontiers in Forests and Global Change, 2022. **5**.
49. Hessl, A.E., et al., *Reconstructing fire history in central Mongolia from tree-rings.* International Journal of Wildland Fire, 2012. **21**(1): p. 86-92.
50. Kolar, T., et al., *Climate and wildfire effects on radial growth of Pinus sylvestris in the Khan Khentii Mountains, north-central Mongolia.* Journal of Arid Environments, 2020. **182**.
51. Kopp, B.J., J. Lange, and L. Menzel, *Effects of wildfire on runoff generating processes in northern Mongolia.* Regional Environmental Change, 2017. **17**(7): p. 1951-1963.
52. Munkhjargal, M., et al., *The Combination of Wildfire and Changing Climate Triggers Permafrost Degradation in the Khentii Mountains, Northern Mongolia.* Atmosphere, 2020. **11**(2).
53. Nasanbat, E., et al. *A fire risk map for protected areas of Mongolia: Dornod Mongol SPA, Numrug SPA, Zed-Khangai-Buteeliin Nuruu SPA and Onon-Balj National Park*. in *Asian Conference of Remote Sensing (ACRS)*. 2020. Deqing, China.
54. Wu, R.H., et al., *Wildfires on the Mongolian Plateau: Identifying Drivers and Spatial Distributions to Predict Wildfire Probability.* Remote Sensing, 2019. **11**(20).
55. Wu, R.H., et al., *Promote the advance of the start of the growing season from combined effects of climate change and wildfire.* Ecological Indicators, 2021. **125**.
56. Zhao, H., et al., *The spatial patterns of climate-fire relationships on the Mongolian Plateau.* Agricultural and Forest Meteorology, 2021. **308**.
57. Bao, Y.L., et al., *Satellite-Based Analysis of Spatiotemporal Wildfire Pattern in the Mongolian Plateau.* Remote Sensing, 2023. **15**(1).
58. Dashpurev, B., et al., *A cost-effective method to monitor vegetation changes in steppes ecosystems: A case study on remote sensing of fire and infrastructure effects in eastern Mongolia.* Ecological Indicators, 2021. **132**.
59. Kazato, M. and B. Soyollham, *Forest-steppe fires as moving disasters in the Mongolia-Russian borderland.* Journal of Contemporary East Asia Studies, 2022. **11**(1): p. 22-45.
60. Li, Y.H., et al., *Risk Factors and Prediction of the Probability of Wildfire Occurrence in the China-Mongolia-Russia Cross-Border Area.* Remote Sensing, 2023. **15**(1).

61. Sainbuyan, B., et al., *Estimation of the burned area with severity and its influencing factors for wildfire using Sentinel-2 satellite imagery: Ой, хээрийн түймрийн шатсан талбай, түүний шаталтын зэрэглэлд нөлөөлөх хүчин зүйлсийн хамаарлын судалгаа.* Geographical Issues, 2023. **23**(01): p. 22-36.
62. Gantumur, B., et al., *A wildfire monitoring study for burn severity and recovery process using remote sensing techniques: A case study near Shiliin Bogd mountain, Eastern Mongolia.* Geographical Issues, 2022. **22**(1): p. 20-31.
63. Boucher, J., et al., *Assessing the potential of the differenced Normalized Burn Ratio (dNBR) for estimating burn severity in eastern Canadian boreal forests.* International Journal of Wildland Fire, 2017. **26**(1): p. 32-45.
64. Cardil, A., et al., *Fire and burn severity assessment: Calibration of Relative Differenced Normalized Burn Ratio (RdNBR) with field data.* Journal of Environmental Management, 2019. **235**: p. 342-349.
65. Gantumur, B., et al., *Implication of urban heat island (UHI) related to human activities: a case study in Mongolia*. SPIE Remote Sensing. Vol. 11157. 2019: SPIE.
66. Parks, S.A., G.K. Dillon, and C. Miller, *A New Metric for Quantifying Burn Severity: The Relativized Burn Ratio.* Remote Sensing, 2014. **6**(3): p. 1827-1844.